AIAA AVIATION Forum
12-16 June 2023, San Diego, CA and Online
AIAA AVIATION 2023 Forum

10.2514/6.2023-3366

Study of Fuel Consumption Reduction Using CoFlow Jet Empennage on B-787-8

Miranda Anhalzer†, Lauren Kendall*, and GeCheng Zha§

Dept. of Mechanical and Aerospace Engineering

University of Miami, Coral Gables, FL, 33124

Abstract

This paper conducts a conceptual design study of the use of CoFlow jet (CFJ) control surface technology on a Boeing 787-8 Dreamliner to allow for high surface control authority with a reduced empennage size. The study evaluates performance metrics of a baseline Boeing 787-8 model and compares the data to the calculated performance and dimensioning of an aircraft with CFJ integrated control surfaces. The study shows the baseline aircraft model validations are in good agreement with published data. The study results show a significant weight and drag reduction on the overall aircraft, with a gross overall weight reduction of 10.24%, and a total drag reduction of 4.65% All these benefits result in an increase of 4.88% of C_L/C_D and a fuel weight reduction of 12.97%. The conceptual study of this paper shows that CFJ-implemented empennage design appears to be a promising technology to substantially reduce the fuel consumption and emission pollution of transonic transports.

---

† Undergraduate Student, Department of Aerospace and Mechanical Engineering.

* Ph.D. Candidate, University of Texas Austin - Department of Aerospace and Mechanical Engineering.

§ Professor, AIAA Associate Fellow.

1. Introduction

Aircraft stability is achieved via the empennage including horizontal and vertical stabilizers. Thus, high control authority with rapid response to maintain aircraft-trimmed stability is essential for aircraft control surfaces. To achieve such performance, control surfaces typically need to be large. This impedes the aircraft's efficiency performance by subsequently affecting the weight, drag, and energy consumption of the aircraft. With aircraft tail sizes having significant effects on aircraft performance, the development of active flow control technology has been widely considered a viable option in allowing for higher control authority to be achieved without the need for a larger tail area. With smaller empennage sizes, significant improvements in fuel efficiency can be achieved.

As of 2019, 23.7% of airlines' operating costs are spent on fuel [1]. With a projected significant increase in commercial air travel over the next few decades, it is expected that the cost of fuel for airlines will also experience a drastic increase. Increasing the fuel efficiency of aircraft is currently one of the biggest priorities for airlines to aid in the reduction of operating costs. This expenditure problem is further exacerbated by the possible adoption of alternative eco-fuels in the future. Biofuels have a lower capital market than traditional jet fuels, therefore they have a much higher overhead cost [34]. There have been certain technological developments with the priority of reducing control surface drag. As mentioned above, active flow control technology has the potential to offer improvements in the aerodynamic efficiency of aircraft. Further analysis of the economic and environmental implications of jet fuel and aircraft fuel efficiency is discussed in the appendix of the paper.

Recent studies [20,18] investigate the use of Active Flow Control (AFC) as a lift enhancement system for aircraft control surfaces [2, 3, 4, 5, 6, 7, 19]. Sweeping jets and synthetic jets are AFC systems used to control the separated flow on vertical tails [19]. These technologies effectively show enhancement in aerodynamic performance alongside the mitigation of flutter [8, 9, 10,11, 12, 13, 14, 15, 16, 18, 20]. Recent research using synthetic jets showed results of a side force increase by up to 18% at moderate rudder deflection and a moment coefficient of $C\mu$=0.721% for a swept and tapered tail with a 29.6% chord rudder [8,20]. The study showed that sweeping jets have a higher $C\mu$ output and corresponding jet velocity than that of synthetic jets. NASA and Boeing performed testing on a full-scale vertical tail model with the use of a 31-sweeping jet actuator configuration [9,10]. This configuration showed significant flow attachment on the rudder, with a 20% increase in the side force at the maximum rudder deflections of 30deg at 0 and -7.5 sideslip angles. These results were further demonstrated and tested in 2015 on the Boeing 757 EcoDemonstrator [20]. From this test flight, it was estimated that with the use of AFC, the side force increased by 13% to 16% at 30 deg rudder deflection for critical sideslip range between β=0 and -7.5.

Active flow control studies are however limited due to insufficient reporting on energy expenditure of the sweeping jets [20,18]. Sweeping jets typically suffer significant energy loss due to flow separation and turning within the actuator. Engine bleed data concerning the energy penalty caused by the introduction of airflow mass is also not presented [20]. In addition to this, when engines are idle, they may be unable to provide sufficient mass flow.

Zhang et al [20,18] conducted a 2D numerical simulation studying the use of Co-flow Jet (CFJ) technology on aircraft control surfaces. The CFJ zero net mass flux (ZNMF) control surface is demonstrated to have low energy expenditure, effectively showing its possible application and effectiveness in significantly reducing the control surface size. Xu et al [21] investigated several techniques to remove drag penalty when the CFJ is not in use. One method found was to allow for the CFJ to produce a light jet on the surface of the airfoil, with this method drag penalties can be mitigated at low energy expenditure. This method was tested at low Mach numbers to simulate cruise speeds and found that in comparison to the baseline, the corrected drag coefficient is decreased by 11.4%,13.0%, and 14.6% at Mach numbers of .15, .45, and .7, respectively [21]. The second method investigated the covering of the injection and suction slot with a movable slot surface. The study found that this method effectively makes the drag coefficient the same as that of the baseline model.

Xu and Zha [18,20] further extend the 2D CFJ control surface to 3D vertical tails. Their studies indicate that it is highly effective to apply CFJ either on the front part of the control surface or the flap. Using CFJ on the flap achieves more control authority at lower energy expenditure, this is due to the use of CFJ technology being advantageous in high adverse pressure gradients [20]. With a significant empennage size reduction, the overall drag and weight of an aircraft can be significantly reduced. These CFJ design implementations have the potential to offer significant weight and drag parameter improvements, offering a significant reduction in fuel consumption for aircraft.

The objective of this paper is to perform a conceptual design and fuel consumption study on the use of flapped CFJ control surface technology on the Boeing 787-8 Dreamliner. With the ability to maintain high control authority with lower control surface size, the empennage size is reduced by 50%, while preserving the baseline flight mission requirements. This paper outlines the design methodology for the aircraft performance and dimensioning calculations of the baseline and CFJ models. The subsequent drag, weight, and fuel consumption changes are calculated and analyzed. An aircraft conceptual design methodology based on Corke [29] and Raymer [30] is adopted for quantifying the baseline and CFJ-aircraft design and performance metrics. Published baseline model performance and design metrics are used to validate the results of the study.

2. CFJ control surface

This section includes further information on the co-flow jet zero net mass flux system, as well as the CFJ control surface data considered and applied in the design of the CFJ B787-8 model in this study.

2.1

Coflow Jet technology is a zero net mass flux control technique that allows for high lift production with a reduction in drag, which is comprised of an injection slot at the leading edge and a suction slot at the trailing edge [20]. A small amount of mass flow is suctioned near the trailing edge slot and compressed by the micro compressor within the airfoil and injected into the leading-edge tangent to the wall surface. Figure 1 illustrates the CFJ airfoil system. In the design of control surfaces, such as vertical and horizontal tails it is important to design a structure that has high control authority.

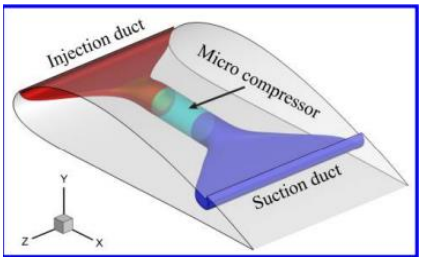

Fig. 1 CFJ Airfoil with Embedded Micro-Compressor Actuator

A numerical study by Xu & Zha [20] showed the use of CFJ technology on the flap of the control surface allows for full flow attachment at a flap deflection angle of up to 70deg. Fig. 2 displays that the baseline control surface at a deflection angle of 30deg has severe flow separation, whereas the control surfaces with CFJ applied on the flap at deflection angles ranging from 30deg to 70deg preserve flow attachment. From the study, the CFJ control surface is able to increase the maximum lift coefficient by three times at the flap deflection angle of 70deg higher than that of the baseline airfoil under the same conditions.

Based on the study of Xu and Zha [20], this paper will conduct a conceptual design study of the benefits of a CFJ-integrated empennage design on the B-787-8. The CFJ empennage design effectively allows for a maximum lift coefficient increase of up to 3 times that of the baseline model. Such a drastic improvement in lift coefficient allows for high control authority to be preserved at 50% reduced empennage size. The CFJ-B787 model will have the same mission requirements as the baseline B787 model including the range, payload, and cruise speed.

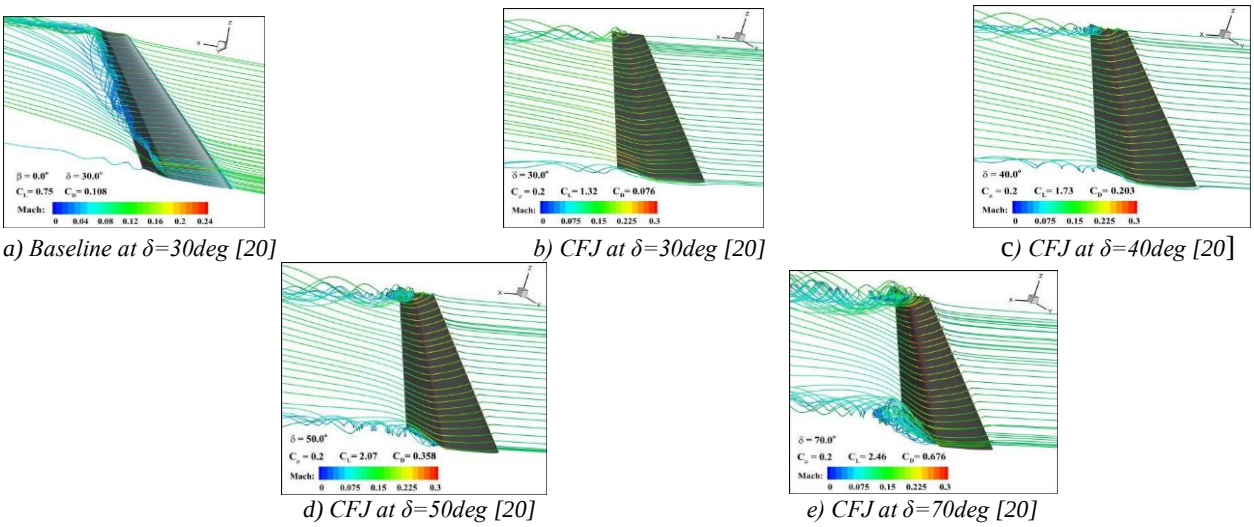

a) Baseline at δ=30deg [20] *b) CFJ at δ=30deg [20]* *c) CFJ at δ=40deg [20]*

d) CFJ at δ=50deg [20] *e) CFJ at δ=70deg [20]*

Fig. 2 Streamlines colored with Mach number showing the separated flow of the baseline control surface at a deflection angle of 30deg and the attached flows of the control surfaces with CFJ applied on the flap at a deflection angle from 30deg to 70deg. [20]

3. B787 Aircraft Design Parameters

The following section outlines the important design methodologies used in the conceptual design of the baseline and CFJ B787 model. These methods are adopted from conceptual design procedures outlined by Corke [29] and Raymer [30]. To ensure accuracy in the design methodologies adopted, the baseline model results are validated using published design and performance parameters, as will be outlined in the result section. Design methodologies not outlined within this section can be found in the appendix.

Performance Parameter	
Max. Mach	0.9
Cruise Mach	0.85
Cruise Alt (ft)	37000
Oper. Rad. (nm)	3677.5
Max L/D	19.62
TSFC Min. (C_{min})	0.506
TSFC Max. (C_{max})	0.506
Engine: Thrust (lbs.)	124800
Aspect Ratio	9.6
Loiter: Time (min)	10
Fuel Reserve (%)	5
Trapped Fuel (%)	1
Structure Factor	0.4959
Payload Non-Exp. (lb.)	53340

Tab. 1 Baseline Aircraft Flight Mission & Performance Parameters

3.1 Take-off weight estimations

The Dreamliner baseline and CFJ model take-off weight are calculated using aircraft and engine performance parameters [29,30]. Optimal take-off weight is found when the initial take-off and final take-off weight lead to a converged solution where the surplus weight is zero. The Take-off and Landing weight iterations serve as the foundation for the various subsections of the aircraft design. The equations and derivations mentioned in this section will be commonly referenced throughout all sections.

The following aircraft flight mission metrics and performance parameters are considered in these calculations. The values below are taken from publicly posted data from Boeing [32,], the engine manufacturer [36], the analysis conducted by Lissys [31], and historical trends of commercial aircraft performance [29,30].

The surplus empty weight of the aircraft can be calculated with the following equation below [29].

$$W_{Surplus\ Empty} = W_{Empty\ available} - W_{Empty\ required} \quad (1)$$

Where the surplus empty weight can be calculated using the empty available weight and the empty required weight (structure weight, fuel weight, payload weight). Optimum aircraft performance occurs when the surplus empty weight is 0. When a surplus weight value of 0 is achieved, the aircraft design is utilizing only the necessary weight needed for the defined flight plan. Eliminating unnecessary surplus

weight ensures that the aircraft's performance is not negatively affected due to the carrying of unnecessary loads.

The weight at each stage in the aircraft flight envelope (as seen in Figure 3) is calculated and can then be used to find the final weight at landing. Various iterations of the calculations noted below are completed to find optimal conditions where the surplus weight is 0. The required mission parameters input for the aircraft weight iteration are the maximum Mach, cruise Mach, cruising altitude, operational radius, the engine's minimum thrust specific fuel consumption, maximum thrust specific fuel consumption, engine thrust, wing aspect ratio, loiter time, loiter altitude, fuel reserve, trapped fuel, and structure factor.

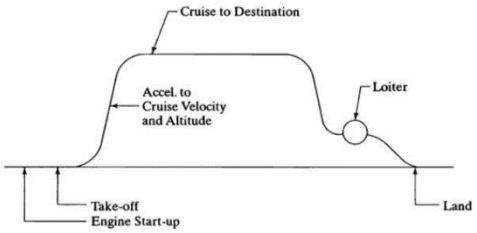

Fig. 3 Aircraft Flight Stages Considered in Weight Iterations [29]

The first stage of the flight envelope includes the startup and take-off of the aircraft. The start-up and take-off weight of the aircraft is calculated using the take-off weight estimation. For the first iteration, an initial estimated take-off weight of 502000 lbs is considered in these equations based on published aircraft performance tables [31,32]. The start-up and take-off stage of the aircraft flight envelope denotes the starting of the engine, taxing, and the aircraft's take-off and initial climb. Based on historical data, an estimation of a 2.5 % weight reduction is caused by the burning of fuel during this rotation [29]. The start-up and take-off weight of the aircraft is thus calculated as 97.5% of the initial take of estimated weight.

$$W_{\text{Start-UP \& T-O}} = W_{\text{TO Estimate}}(1 - .025) \tag{2}$$

After the start and take-off rotation, the aircraft climbs to a cruising altitude and accelerates to cruise speed. Similarly, to the weight derivation seen above, during this stage, the aircraft experiences a reduction in weight due to the burning of fuel. The weight fraction for this part of the climb can be estimated using empirical aircraft data- the following figure illustrates the weight fraction values in relation to cruising Mach numbers. Referencing Figure 4, with a cruise Mach of .85, it is deduced that 3% of the weight is decreased due to fuel burning, and a weight fraction of .97 is used for the climb weight calculations.

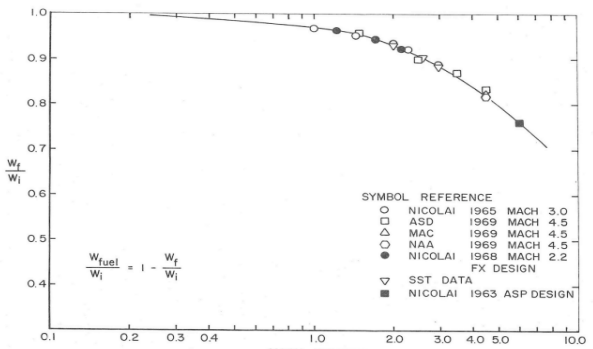

Fig. 4 Weight Fraction for Different Aircraft Cruise Mach Numbers [29]

$$W_{\text{Climb}} = W_{\text{Start-Up \& TO}}(1 - .03) \tag{3}$$

Following the climb to the cruise stage, the aircraft enters cruising conditions. While the aircraft is in cruise it is experiencing unaccelerated steady-level flight. The cruising weight is calculated using the following equation.

$$W_{\text{Cruise}} = \frac{W_{\text{Climb}}}{e^{\frac{R*6080*\frac{C_{\min}}{V*\frac{L}{D}*3600}}{}}} \tag{4}$$

The Boeing 787-8 aircraft in this study utilizes a twin turbojet propulsion system. The weight estimation during cruising conditions (steady unaccelerated flight) is calculated using the Breguet range equation for turbojet engines.

$$R = \frac{V}{C} * \frac{L}{D} ln\left(\frac{W_i}{W_f}\right) \quad (5)$$

R is the range in nautical miles, which is considered twice the value of the operational radius (this being to account for flight to destination and flight back to starting location). The remaining variables considered are as follows: V is the cruise velocity, C is the thrust-specific fuel consumption, and (L/D) is the lift-to-drag ratio during cruise. For most fuel-efficient results lift-to-drag ratio is estimated as 94% that of the maximum L/D per historical aircraft design methodology [29].

$$\frac{\mathrm{L}}{\mathrm{D}} = .94\left[\frac{\mathrm{L}}{\mathrm{D}}\right]_{\max} \quad (6)$$

Equations (5) and (6) can be placed into equation (4) to find the weight at cruise.

The loiter portion of the flight accounts for a limited-time cruise around the landing site, typically reserved for possible delays due to air traffic. The fuel weight fraction for this phase is derived from the loiter endurance equation for the aircraft. Using the aircraft's initial weight ($\mathrm{W_{Cruise\ back}}$) and final weight ($\mathrm{W_{Loiter}}$), the plane's endurance can be calculated.

$$\mathrm{E} = \frac{1}{\mathrm{C}} * \frac{\mathrm{L}}{\mathrm{D}} \ln\left(\frac{\mathrm{W_{cruise\ back}}}{\mathrm{W_{Loiter}}}\right) \quad (7)$$

The endurance denotes the flight time the aircraft is loitering. Rearranging this formulation, the loiter weight can be found.

$$W_{Loiter} = \frac{W_{Cruise\ back}}{e^{E*\frac{C_{min}}{\frac{L}{D}*60}}} \quad (8)$$

The weight at landing can be found using the same empirical weight fraction estimation used for start-up and take-off. Referencing back to Figure 4, an estimated 2.5% of weight decrease due to the burning fuel is estimated.

$$W_{land} = W_{Loiter}(1 - .025) \quad (9)$$

With the weight of the aircraft at all flight stages calculated, the total fuel weight can be found. The take-off weight is subtracted by the weight at landing. This value is added with the 6 percent of the initial allocated fuel weight (which includes the 5% reserve fuel and 1% trapped fuel.)

$$W_{fuel} = (W_{Take-off\ estimate} - W_{Land}) * 1.06 \quad (10)$$

The available empty weight and required empty weight can then be calculated. The payload weight is estimated as the total weight contribution of passengers and personnel (including luggage and non-aircraft equipment) and can be found in Table 1.

$$W_{Available} = W_{Take-off\ estimate} - (W_{Payload} + W_{Fuel}) \quad (11)$$

The required weight denotes the structure weight of the aircraft. To find this value, the initial estimated take-off weight is multiplied by the structure factor (as found in Table 1).

$$W_{Required} = W_{Take-off\ estimate} * s \quad (12)$$

The calculated take-off weight can then be calculated using the payload weight, and equations 12 and 10.

$$W_{Take-off\ calculated} = W_{fuel} + W_{Empty\ Required} + W_{Payload} \quad (13)$$

With the derived take-off weight calculated, it can then be input back into equation 2 to continue the weight iterations. The iterations are continued until the surplus weight is 0.

$$W_{Surplus\ Empty} = W_{Empty\ available} - W_{Empty\ required} = 0 \tag{14}$$

3.2 Tail Design Calculations

The tail is essential for the stability, control, and maneuverability of the aircraft. Similar to many commercial transport aircraft, the B787-8 has a conventional tail design. The horizontal stabilizer offers stability by creating lift that counteracts lift forces produced by the wing and fuselage, thus allowing for an aircraft to be trimmed (referring to when the aircraft is statically stable). In addition to this, the horizontal tail enables aircraft control via the pitching of the elevators. Through this process, the angle of attack of a plane can be adjusted. The vertical stabilizer acts as a critical component in enabling the maneuverability of the aircraft. Adjustments of the vertical stabilizer angle allow for a pilot to control the yawing of the aircraft.

Due to all the factors discussed above, the accurate design of the empennage is imperative in ensuring optimized and safe aircraft operations. To allow for efficient control and stability, the empennage is designed in relation to the wing and fuselage dimensioning as well as the mission requirements (Table 1). Using published aircraft data and historical trends [25,29,30,31,32,36], the following design parameters are used for the vertical and horizontal stabilizer dimensioning for the baseline model.

Vertical Tail Design Parameter	
C_{VT}	.08
l_{vt} (ft)	77
Λ (deg)	40
t/c	.12
λ	.22
A_{vt}	1.7
b_w (ft)	197.3
S_w (ft^2)	4058

Tab. 2 Baseline Vertical Tail Design Parameters

Horizontal Tail Design Parameter	
C_{HT}	.90
l_{ht} (ft)	81.8
Λ (deg)	36
t/c	.12
λ	.22
A_{ht}	5
b_w (ft)	197.3
S_w (ft^2)	4058

Tab. 3 Baseline Horizontal Design Parameters

3.2.1 Vertical Tail Sizing

In the vertical tail design, a vertical stabilizer scaling coefficient (C_{VT}) based on the tail volume ratio is used. This coefficient can be deduced via historical aircraft trends. Historical trends for similarly sized commercial jet transport aircraft are used. With the C_{VT} value equating to .08 [29].

$$S_{VT} = C_{VT} * \frac{b_w s_w}{l_{vt}} \tag{15}$$

The main wingspan (b_w) and wing area (s_w) are used for the sizing of the vertical stabilizer. The variable l_{vt} denotes the distance between the quarter chord locations of the mean aerodynamic chord ($m.a.c$) of the vertical stabilizer and wing [29].

3.2.2 Horizontal Tail Sizing

Similar methodology used for the vertical tail sizing is utilized for the aft stabilizer area. The horizontal tail sizing is based on the horizontal stabilizer scale coefficient (C_{HT}). A value of .90 for the horizontal coefficient is deemed appropriate based on historical data [29].

$$S_{HT} = C_{HT} * \frac{\bar{c}_W s_w}{l_{ht}} \tag{16}$$

The mean aerodynamic center of the main wing and the distance between the quarter chord locations of the *m.a.c* of the main wing and horizontal stabilizers are used (l_{ht}) [29]. The variable $\bar{c}_W$ denotes the *m.a.c* location of the main wing in reference to its respective leading edge. This value can be calculated using the wing's root chord length (c_r) and taper ratio (λ).

$$\bar{c}_W = \frac{2*c_r}{3}\left[\frac{1+\lambda+\lambda^2}{1+\lambda}\right] \tag{17}$$

3.2.3 Tail Design

The Boeing 787-8 aircraft has a conventional tail configuration thus the conventional aspect ratio equation can be used to find the tail span. The aspect ratios considered in these calculations are estimated from historical aircraft design trends [31]. For the horizontal ($\boldsymbol{A}_{ht}$) and vertical ($\boldsymbol{A}_{vt}$) tail aspect ratios, values of 5 and 1.71 are used, respectively.

$$A = \frac{b^2}{S} \tag{18}$$

Rearranging equation 20 allows for the calculation of each tail component's tail span.

The tails planform shape can further be defined through the calculations of root (C_r) and tip chords (C_t) lengths. For both the horizontal and vertical stabilizer, these values are calculated using their respective dimensioning as calculated in the previous tail design sections and the design parameters found in Tables 2 and 3.

$$C_r = \frac{2b}{A(1+\lambda)} \tag{19}$$

$$C_t = \lambda C_r \tag{20}$$

3.3 Tail and Wing Drag Calculations

This section outlines the equations considered to calculate the drag of the tail and wing components. The methodology for calculating the fuselage drag can be found in the appendix.

Quantifying the drag contribution of the empennage and wing components is vital in understanding the aircraft's performance. For the purpose of this paper, each components drag is quantified using viscous drag calculations which relies on a form factor to consider the pressure drag. To find the viscous drag of each component, certain terms and values need to be defined. The following equations are used to find the drag contributions of each component. These calculations can be applied to the wing, vertical tail, and horizontal tail using their respective dimensioning and sizing.

$$V_{eff} = V_\infty * cos\left(\Lambda_{LE} * \frac{\pi}{180}\right) \tag{21}$$

$$q_{eff} = .5 * \rho_{cruise} * V_{eff}^2 \tag{22}$$

$$Re_{m.a.c} = m.a.c\left(\frac{V_{eff}}{\mu/\rho}\right) \tag{23}$$

The effective velocity (V_{eff}) ,is an airplanes speed in relation to the fluid speed. This value acts as a comparison to the freestream velocity (V_∞). The μ/ρ represents the ratio between the dynamic viscosity and density at cruising conditions. The effective velocity is important for calculating the effective dynamic pressure (q_{eff}) and the Reynolds number of the flow ($Re_{m.a.c}$). These values are used to find the friction coefficient for each respective structure, which allows for viscous drag calculations to be completed.

The effective Mach number is similarly defined and is of equal importance in the viscous drag calculations.

$$M_{eff} = M * cos\left(\Lambda_{LE} * \frac{\pi}{180}\right) \tag{24}$$

Where $\Lambda_{LE}$is the leading-edge sweep angle. The friction coefficient is used for the calculation of viscous drag on the surface of the structure. Depending on the development length of the flow boundary layer, the

friction coefficient (cf) can be calculated for laminar and turbulent flow. It is important to note that for commercial aircraft it is typically assumed that the flow will be turbulent.

$$cf = \frac{1.328}{\sqrt{Re_x}} : laminar \tag{25}$$

$$cf = \frac{.455}{(log_{10} * Re_{m.a.c})^{2.58}(1 + .144 * M^2{}_{eff})^{.65}} : turbulent\ (\sqrt{Re_x} \geq 1000) \tag{26}$$

The form factor (F) is used to quantify pressure drag and the flow separation effect [29].

$$F = \left[1 + \frac{.6}{\left(\frac{x}{c}\right)_m}\left[\frac{t}{c}\right] + 100\left[\frac{t}{c}\right]^4\right]\left[1.34M^{.18}\left(cos\ cos\ \left(\Lambda_{\frac{t}{c}max}\right)\right)^{.28}\right] \tag{27}$$

With the form factor and friction coefficient calculated, the parasitic drag, $C_{d_\circ}$, is calculated. The variable Q denotes the interference factor. This factor aims to estimate fuselage and wing interference influence in increasing the base drag. An interference factor of .95 is deemed appropriate based on historical data of aircraft with similar wing-fuselage arrangements [29].

$$C_{d_\circ} = \frac{C_f * S_{wet} * F * Q}{S} \tag{28}$$

It is important to note that S_{wet} denotes the wetted surface area of the respective wing or tail component.

$$S_{wet} = 2.003 * S \tag{29}$$

Using the parasitic drag coefficient value, the drag is calculated.

$$D = C_{d_\circ} * q * S \tag{30}$$

For these calculations, the variable S , represents the area of the wing, vertical tail, or horizontal tail depending on which component's drag is being calculated. These drag calculations are completed for the wing and stabilizers using their respective design parameters.

3.4 Tail Structure Weight

The horizontal and vertical tail weight is calculated using the aircraft's design dimensions and parameters at cruising conditions [29,30]. Many of the values used in the following equations have been either calculated or used in previous sections.

The fuselage width at the location of the vertical stabilizer is represented by Fw. The design gross weight, W_{dg}, is taken from the optimized final take-off weight found via the iterations discussed in section 3.1. The design load factor, n, is used to represent the loads an aircraft is expected to experience during normal flight condition operations [29,30]. Typically, design loads are found in specific design and operations manuals for aircraft. Because such documents for the B787-8 are not available, an estimation for the load factor is made considering historical trends for similar aircraft [29]. A value of 2.5 is assigned for the design load factor. The pitching radius of gyration, K_y, is calculated proportionally to the l_{ht}.

$$K_y \approx .3 l_{ht} \tag{31}$$

With the above variables defined, the horizontal tail weight is calculated with the formulation as follows.

$$W_{Htail} = .0379(1 + Fw/b_{ht})^{-.25}(W_{dg})^{.639}(n)^{.1}(S_{ht})^{.750}(l_{ht})^{-1}(K_y)^{.704}(cos\ (\Lambda_{HT}))^{-1}(A_{HT})^{.116} \tag{32}$$

For the vertical tail weight estimations, the following values are considered. The $\frac{H_T}{H_v}$ represents the ratio between the horizontal tail's root chord's height above the fuselage centerline and the tail tip chord's distance from the fuselage centerline. H_v is assumed to be the same value as the vertical tail span. The horizontal tails root chord is assumed to be in line with the fuselage centerline, therefore the value for $\frac{H_T}{H_v}$ is calculated to be zero. The yawing radius of gyration is estimated to have the same value as the L_{vt}. The variable K_{rht} is used as a coefficient to define distinct types of tails. For conventional non-fighter aircraft, this coefficient value is 1.

$$W_{Vtail} = .0026K_{rht}(1+\frac{H_T}{H_v})^{.225}(W_{dg})^{.556}(n)^{.536}(S_{VT})^{.5}(L_{VT})^{-.5}(K_Z)^{.875}(cos\ (\Lambda_{VT}))^{-1}(A_{VT})^{.35}(\frac{t}{c})^{-.5} \quad (33)$$

A comprehensive weight analysis for other structural components of the aircraft is conducted in this study. The equations and methodology used for these calculations not included in this section can be found in the appendix.

4. CFJ B787 Design

Due to the implementation of the CoFlow jet technology into the empennage, additional design considerations are necessary. With a decreased empennage size, it is imperative to ensure stability and control functions of the aircraft are preserved. In addition to this, because of a 50% reduction in empennage size, the CFJ model design needs to compensate for overall structural size and weight reductions. Higher aerodynamic efficiency and reduced takeoff weight must be considered within the conceptual design. Another vital parameter discussed is that of the CFJ component weight and power consumption.

This section lists the important parameter design and considerations for CFJ B787 design. The CFJ's model sizing calculations, CFJ component weight and power calculations, and stability verification are outlined within the section.

4.1 CFJ Aircraft sizing

4.1.1 Tail Sizing

In this study, the performance of a 50% reduced empennage aircraft is analyzed for the CFJ-B787-8. The following equations are used in the scaling of the CFJ B787's tails. These equations are considered for both the vertical and horizontal tail.

$$S_{Tail\ CFJ} = \frac{1}{2}S_{Baseline} \quad (34)$$

$$B_{Tail\ CFJ} = \frac{1}{2}B_{Baseline} \quad (35)$$

As has been previously mentioned, the CFJ model's tail is uniformly scaled down by ½ . Each tail's respective aspect ratio is then calculated as follows.

$$A_{Tail\ CFJ} = \frac{{B_{Tail\ CFJ}}^2}{S_{Tail\ CFJ}} \quad (36)$$

4.1.2 Wing Sizing

A decrease in the size of the empennage will impact the overall wing sizing requirements for efficient and safe aircraft operations. A 50% scaled down tail design will lead to a decrease in the weight and drag of the overall structure. With a reduced weight during take-off conditions, the aircraft will not require the same sized wings as that of the baseline model. With the wing retaining the same aerodynamic performance parameters, less lift will need to be produced to maintain cruising conditions.

The wing loading calculations of the aircraft can be used to calculate the CFJ aircraft model's wing sizing and dimensioning. Referencing back to the take-off weight calculations section, the weight at the time of start to cruise for the CFJ model is used. Assuming the wing loading at this stage of the flight mission remains constant for both the CFJ and baseline model, the wing area for the CFJ can be found.

The wing loading is found using the parasitic drag coefficient, the dynamic pressure, the aspect ratio, and the wing efficiency factor (e). The Oswald efficiency factor can typically be assumed to be approximately .8. [29]

$$\frac{W}{S}_{Baseline} = \sqrt{\frac{C_{d_\circ}}{2(\frac{1}{\pi eA})}} * q \quad (37)$$

$$S_{CFJ\ Model} = W_{CFJ\ Cruise-Start} \div \frac{W}{S}_{Baseline} \quad (38)$$

The wingspan of the wing is calculated using the same aspect ratio for the baseline model's wing. As seen in Table 1, the aspect ratio considered for these calculations is 9.6.

4.2 CFJ System Weight and Power Calculations

The CFJ actuator system weight and performance estimations are calculated using the published data on the delayed detached eddy simulation study investigating the performance of 3D aircraft control surface with a Coflow Jet active control system [20].

Cases	C_μ	C_L	ΔC_L	C_D	P_c	C_L/C_D	$(C_L/C_D)_c$	$\Delta(C_L/C_D)_c$	Γ
Baseline EXP [61]		0.78	-	0.112	-	6.96	6.96	-	-
Baseline CFD	-	0.75	-	0.108	-	6.93	6.93	-	-
Front CFJ	0.025	0.96	28.1%	0.109	0.026	8.84	7.09	2.3%	1.02
Flap CFJ	0.025	1.095	46.1%	0.113	0.005	9.65	9.24	33.1%	1.006
Flap CFJ	0.05	1.166	55.5%	0.115	0.017	10.16	8.85	27.5%	1.013
Flap CFJ	0.1	1.234	64.5%	0.104	0.054	11.89	7.79	12.1%	1.030
Flap CFJ	0.2	1.323	76.4%	0.076	0.217	17.35	4.51	-35.0%	1.083
Flap CFJ	0.26	1.365	82.0%	0.056	0.461	24.36	2.64	-62.0%	1.154

Tab.4 Aerodynamic performance of the control surface with different Cμ [20]

A moment coefficient,C_u, of .1 is selected for this design study. Referencing Table 4, a corresponding power coefficient P_c of .054 is found. The Power coefficient is expressed as:

$$P_c = \frac{P}{\frac{1}{2}\rho_\infty V_\infty^3 S_{Tail}} \tag{39}$$

$$P_{CFJ-act} = P_{CFJ}/\eta \tag{40}$$

The actual power P_{act}, can be calculated, where η is the CFJ micro-compressor actuator efficiency. In this paper, a conservative value of 75% is used. A typical efficiency in the range of 78%-82% can be achieved. The free stream density value is taken at sea level conditions. It is important to note the free stream velocity value used equates to that of the take-off velocity. The area as denoted above accounts for the empennage tail area.

$$V_{TO} = 1.2V_{stall} \tag{41}$$

$$V_{stall} = \sqrt{\frac{2W}{\rho S C_{Lmax}}} \tag{42}$$

A conservative power density of 3 kw/kg is used for weight and power calculations for the CFJ components in the empennage. The weight of the CFJ in the vertical and horizontal stabilizers can be calculated as seen below. A value of 2.205 lb. is used as a conversion factor to convert the calculated mass in kg to weight.

$$W_{CFJ} = \frac{P_{CFJ-act}}{P_d} * 2.205 \tag{43}$$

The calculated weight contributions for the CFJ component weight can be found in the CFJ B-787-8 results section.

4.3 Aircraft Stability Validation

With a decrease in structural size and weight of the empennage component, stability validations are necessary to ensure static stability for the aircraft assembly. Using the aircraft component weights and center of lift location, calculations are completed to ensure static stability of the CFJ model is preserved. Both longitudinal and lateral stability must be analyzed to ensure appropriate stability and control requirements for the model.

The longitudinal stability of an aircraft can be found by quantifying the loads acting upon the structure [29,30]. The load summary of the fuselage can be calculated using the magnitude of all aircraft loads (including structures and payload), as well as the spanwise regions in which these load act. For the

purpose of this stability validation- the weight contribution of the fuel, payload, fuselage, wing, engines, tail, landing gear, nacelle group, seats, anti-ice system, avionics, air conditioning, flight control system, engine control system, and hydraulics are considered. These values can be used to calculate each respective moment acting on the center of lift. The center of lift is estimated to be at the ¼ location of the mean aerodynamic chord. The spanwise region in which these loads act can be calculated using their respective starting and ending location in relation to the length of the fuselage structure (x/l). Using these conventions, the loads are assumed to be uniformly distributed. The resultant x/l value for each load is calculated using the following relation.

$$\frac{x}{l} = .5 * \left[\left(\frac{x}{l}\right)_{end} - \left(\frac{x}{l}\right)_{start}\right] + \left(\frac{x}{l}\right)_{start} \tag{44}$$

With the resultant load distribution and load magnitude (F_y) calculated, the moment acting on the aircraft center of lift is calculated.

$$M_{CoL} = F_y * \left(\frac{x}{l} - l_{ctr}\right) * l \tag{45}$$

For this study, the center of lift (l_{ctr}) is assumed to be ¼ the length of the mean aerodynamic chord. The total moment acting on the center of lift of the structure can be found by summing all respective moment calculations for every load.

$$\sum M_{CoL} = \sum M_{CoL} components \tag{46}$$

With the total moment acting on the center of lift calculated, the aircrafts resultant center of gravity can be found. The following equation can be calculated using the center of lift location, the length of the fuselage, and the resultant load acting on the structure.

$$X_{cg} = \frac{\sum M_{CoL}}{\sum F_y} + (l_{ctr} * l) \tag{47}$$

The static margin of the aircraft can be calculated using the following relation.

$$S.M. = (l_{ctr} - \frac{X_{cg}}{l}) * \frac{l}{m.a.c} \tag{48}$$

The following relations dictate the stability status of the aircraft.

$$If \quad S.M > 0 \ \therefore Stable$$
$$If \quad S.M < 0 \ \therefore Unstable$$

Directional stability is also critical for optimum and safe flight operations. Directional motion describes the rotation of the aircraft about its vertical axis. The rotational movement is directly produced by the fuselage and wing of the structure. The vertical tail is essential to oppose this rotational motion by producing a counter slip vector. The counter moment produced by the vertical stabilizer effectively reduces the side slip angle, β, and allows for the aircraft to maintain its flight direction. The directional stability of an aircraft structure can be found using the sum of the wing, fuselage, and tail directional stability coefficients.

The following equation quantifies this value using the wing and vertical tail dimensions, the height of the wing's root chord in relation to the fuselage centerline (zw), and the total height of the fuselage (h).

$$\frac{\left(1 + \frac{d\sigma}{d\beta}\right) qvs}{q} = .724 + \frac{\frac{3.06 S_{vt}}{S_w}}{1 + \cos\left(\Lambda_{vt} * \frac{\pi}{180}\right)} + .4\frac{zw}{h} + .009 A_w \tag{49}$$

With the quantified fuselage and wing influence on the horizontal stabilizer, the vertical stabilizer's directional stability can be calculated. The vertical tail volume coefficient is used in this calculation and is defined below.

$$\overline{V_{vs}} = \frac{l_{vt} s_{vt}}{b_w s_w} \tag{50}$$

Using the tail volume coefficient and $C_{L_\alpha} = \frac{dC_L}{d\alpha}$, the vertical tail directional stability coefficient is calculated.

$$(C_{n_\beta})_{vt} = \overline{V_{vs}}(C_{L_\alpha})_{vs} * \frac{180}{\pi}[\frac{\left(1 + \frac{d\sigma}{d\beta}\right) qvs}{q}] \tag{51}$$

The fuselage directional stability coefficient is calculated using the fuselage volume, fuselage height (h) and width (w) measurements, as well as the aircraft's wings dimensions.

$$(C_{n_\beta})_F = -1.3\frac{(VOL)_F}{S_w b_w}\frac{h}{w} \tag{52}$$

The aircraft wing's contribution to the directional stability is calculated as seen below.

$$(C_{n_\beta})_w = {C_L}^2[\frac{1}{4\pi A_w} - \frac{\tan\left(\Lambda_w * \frac{\pi}{180}\right)}{\pi A_w\left(A_w + 4\cos\left(\Lambda_w \frac{\pi}{180}\right)\right)}(\cos\left(\Lambda_w \frac{\pi}{180}\right) - \frac{A_w}{2} - \frac{A_w^2}{8\cos\left(\Lambda_w \frac{\pi}{180}\right)} + \frac{\frac{6x}{\bar{c}}\sin\left(\Lambda_w \frac{\pi}{180}\right)}{A_w} \tag{53}$$

$$C_{n_\beta} = (C_{n_\beta})_w + (C_{n_\beta})_F + (C_{n_\beta})_{vs} \tag{54}$$

The equation above effectively accounts for the destabilizing effects of the fuselage, wing, and vertical stabilizer. Based on historical data, a reasonable range for the directional stability coefficient can be deduced using the cruising Mach number of the aircraft [29,30]. Accounting for the cruising Mach of .85, the following range is selected for lateral stability analysis of the aircraft.

$$.08 \leq C_{n_\beta} \leq .25 \tag{55}$$

A more precise tail drag contribution can be calculated considering the stability equations discussed above. The tails drag contribution was discussed in previous sections; however, these calculations are limited to only considering the parasitic drag contribution. Having found the aircraft's center of gravity and tail volume ratio, an estimate for the horizontal tail lift coefficient during cruising conditions can be estimated.

$$C_{M,cg} = C_{M,ac,W} + C_{L,W}(h - h_{ac,W}) - V_{ht}C_{L,t} \tag{56}$$

where $h - h_{ac,W}$ is the distance between the aircraft center of gravity and neutral point normalized by the wing chord. The tail lift coefficient can be estimated assuming that the above equation is solved under trimmed aircraft conditions- where the moment coefficient about the center of gravity is zero. The wing trim lift coefficient is used. Due to the unavailability of wind tunnel testing data for the aircraft, the airfoil profile data is used to estimate the moment coefficient of the wing about the aerodynamic center, $C_{M,ac,W}$ [30]. Using the moment coefficient vs. angle of attack graphs for the NASA SC 0714 airfoil and the wing design parameters, this value can be estimated.

$$C_{mac,W} = \frac{C_{M,0}\left(A_w * cos^2\left(\Lambda_w * \frac{\pi}{180}\right)\right)}{(A_w + 2 * \cos\left(\Lambda_w * \frac{\pi}{180}\right))} \tag{57}$$

Rearranging equation 57 yields a formulation for the horizontal tail during trim conditions.

$$C_{L,t} = (C_{M,ac,W} + C_{L,W}(h - h_{ac,W}))/V_H \tag{58}$$

Knowing the lift coefficient for the tail allows for the calculation of the lift induced drag produced by the horizontal stabilizer. The aspect ratio and Oswald efficiency factor are considered for the lift induced drag coefficient calculation. It is important to note that for the baseline model an efficiency of .8 is typically deemed reasonable. Due to the performance of CFJ technology, an efficiency factor ranging from .8 to 1 can be considered for the CFJ model.

$$C_{Di} = \frac{C_{L,t}^2}{\pi e A} \tag{59}$$

Using the drag polar equation this value can be summed with the previously calculated parasitic drag to find the total drag produced by the horizontal stabilizer.

$$C_D = C_{D0} + C_{Di} \tag{60}$$

5. Results

5.1 Design Methodology Validation Results

To verify the design methodology applied in this paper (as seen in section 3.1-3.4), the results calculated for the B787-8 baseline model are compared with published data found from various reputable sources. Sizing and design parameters published by the manufacturer (Boeing) are prioritized within this analysis. However, due to the nature of several Boeing design metrics being private proprietary information, other sources are considered within this validation study. In addition to publicly available data posted by Boeing and airline partners [32,25], the aircraft design analysis completed by Lissys Ltd. [31] is considered. Lissys published a comprehensive design and performance analysis of the B787-8 in conjunction with their performance analysis software, PianoX. The subscript within the table below acts as an identifier for the source of the published data considered.

The percentage difference between the calculated metrics within this study and published values are calculated using the following equation.

$$Percent\ Difference = \frac{|V_{Study} - V_{Published}|}{\frac{V_{Study} + V_{Published}}{2}} * 100 \tag{61}$$

Parameter	Calculated B787-8 Data	Published Data	Percent Difference
WTO ($lb.$)	502499.18	502500	<0%
Structure weight ($lb.$)	243009.62	242000	1.5%
Horizontal tail area (ft^2)	943	832.5*	12.45%
Horizontal tail span (ft)	68.7	65	5.53%
Vertical tail area (ft^2)	416	427.5 *	2.73%
Vertical tail span (ft)	26.6	26.96*	1.34%
Vertical Tail Weight ($lb.$)	2456.18	2138*	13.85%
Horizontal Tail Weight ($lb.$)	4942.82	5158*	4.26%
*** Lissys Ltd. [31]**	**Boeing [32,36,25]**		

Tab. 5 Validation for Design Methodology with Published Data

Table 4 shows a reasonable agreement between the calculated values with the published values found. All but two measured values are within a 5% range of difference when compared to published data. The design parameters with the highest percent difference to published values are the horizontal tail area and vertical tail weight. These parameters showed a 12.45% and 13.85% difference from published results.

This conceptual design study relies heavily on historical data to make inferences on certain aircraft sizing and scaling requirements. Because of this, it is possible that some of the sizing discrepancies are due to a lack of access to precise data for the B787-8. Considering this limitation, the validation analysis showed reasonable agreement between the calculated and published values. It can be concluded that the design methodology used within this study is reasonable and acceptable.

5.2 CFJ B-787-8 Performance and Design Analysis

5.2.1 Aircraft Sizing Results and Analysis

The major design parameters discussed within this paper are those of the aircraft tail and wing sizing. The empennage component experienced a total size reduction of 50%, as is found in equations 34 and 35. Because of a reduction in empennage size and subsequently the total structure weight of the aircraft, a reduction in wing sizing is deemed acceptable and expected. Using the aircrafts wing loading at cruise, the CFJ model's wing sizing is calculated as can be seen in equation 37. Table 6 below outlines the major design sizing parameters found and calculated for the baseline and CFJ B787-8 models.

Parameter	Baseline-B787	CFJ-B787	Percent Change
S wing (ft^2)	4058.00	3642.63	-10.24%
b wing (ft)	197.37	187.00	-5.25%
S_{ht} (ft^2)	943	472	-50%
b_{ht} (ft)	68.7	34.4	-50%
S_{vt} (ft^2)	416	208	-50%
b_{vt} (ft)	26.6	13.3	-50%

Tab.6 Baseline B787-8 and CFJ B787-8 Model Sizing

Per the objectives of this study, the empennage components experienced a 50% size reduction for the CFJ model. The CFJ model's wing area experienced a total reduction of 10.24%. As previously mentioned, this calculation is derived via the wing loading of the aircraft. The effects of the aircraft sizing reductions are further shown in the following section where the weight values for the CFJ and baseline model are outlined.

5.2.2 Aircraft Weight and Performance Results and Analysis

With the CFJ integrated empennage, the CFJ Boeing 787-8 aircraft has a significant weight reduction as well as improved performance metrics. Table 7 and 8 below present the important weight and performance results found in this study.

Parameter	Baseline-B787	CFJ-B787	Percent Change
WTO $(lb.)$	502499.18	451064.26	-10.24%
Total Fuel $(lb.)$	199969.84	174041.28	-12.97%
Required Empty Weight $(lb.)$	246189.3387	223682.9764	-10.24%

Tab.7 Baseline B787-8 and CFJ B787-8 Models Weight Performance Results

The 50% reduced CFJ integrated empennage design has significant effects on the total weight and fuel consumption of the aircraft. As previously discussed, the wing experiences a size reduction which subsequently decreases the total weight contribution of the wing structure. Similar weight reduction effects occur throughout other aircraft sizing components due to reductions in the tail and wing sizing's as well as reductions in take-off and landing weights. The methodology used for in-depth structure weight calculations can be found in the appendix. The CFJ-B-787-8 model has a 10.24% reduced gross and structure weight, and a 12.97% reduced fuel weight.

With a reduction in aircraft structure sizing and weight, the following aerodynamic parameters are found.

Parameter	Baseline-B787	CFJ-B787	Percent Change
L/D	19.62	20.58	4.88%
CL	0.50159	0.50159	0.00%
CD	0.02557	0.02438	-4.65%
CDo	0.01496	0.01376	-8.03%
CD nacelle	0.00060	0.00053	-11.57%
CD trim	0.00020	0.00019	-4.35%
CDo Empennage	0.00535	0.00268	-50%
CDi Empennage	0.00002	0.00019	950%
CL Empennage	.017	.035	205.88%
CD Empennage	0.00537	0.00287	-46.55%

Tab.8 Baseline B787-8 and CFJ B787-8 Models Aerodynamic Performance Results

The aerodynamic efficiency of the CFJ model experienced an increase of 4.88%. This can be attributed due to the decrease in overall weight and structure size of the CFJ model. The parasitic drag of the horizontal stabilizer is decreased as quantified in section 3.4.1.The lift induced drag coefficient, as calculated in section 4.3, increased for the CFJ model. This can be observed by the horizontal tail lift coefficients values. The CFJ model yielded higher results for the tail lift coefficient during trimmed conditions, this is because higher tail lift is needed to maintain longitudinal stability with a reduced empennage size. Due to the lift enhancing effects of the CFJ technology, the increased tail lift coefficient of the CFJ model can be achieved. The higher lift induced drag does not significantly affect the overall drag produced by the tail components. The total drag reduction for the CFJ model is largely attributed to the significant tail planform area size reduction. The study found a calculated drag reduction of 46.55% for the CFJ model.

5.2.4 Tail Weight Results and Analysis

The following table compares the empennage structure weight between the baseline and CFJ models.

Component	Baseline Model	50% CFJ Model	Percent Change
Horizontal Tail (lb.)	4942.82	2408.12	-50.94 %
Vertical Tail (lb.)	2456.18	1283.25	-47.75 %

Tab.9 Baseline B787-8 and CFJ B787-8 Empennage Weight

As seen in the table above, The CFJ B787-8 model design yielded a total empennage weight reduction by approximately 50%. Added weight due to the implementation of the CFJ subsystem must also be considered. At a conservative 75% CFJ efficiency, the power values for the vertical and horizontal stabilizers are calculated to be 542.02 kW and 1228.67 kW, respectively. The horizontal and vertical CFJ component weight calculations yield a result of 891.43 lb. and 393.25 lb. With the CFJ subsystems considered, the horizontal and vertical tail weights still yield significant weight reductions of 32.4 % and 31.9% respectively.

The following figure illustrates the 50% empennage size reduction for the CFJ B787-8 Model.

Fig. 8 B-787-8 Baseline and CFJ Model Comparison with 50% Empennage Reduction

5.3 Stability validation and Analysis

With a decreased empennage structure size and weight, the stability of the aircraft is analyzed to ensure sufficient static stability. As mentioned in earlier sections of this paper, aircraft stability is maintained if the following conditions are met.

Longitudinal Stability $S.M > 0$

Directional Stability $.08 \leq C_{n_\beta} \leq .3$

The following table presents the longitudinal and directional stability coefficients for the baseline and CFJ models.

Directional	Baseline Model	50% CFJ Model
Longitudinal Static Margin	.18	.24
Directional Stability Coefficient	.09	.10

Tab.10 Baseline and CFJ Aircraft Models stability Coefficients

The above results confirm that longitudinal and directional aircraft stability are preserved in the CFJ aircraft model with reduced empennage sizing. It's important to note that the calculations done specifically for the longitudinal stability relied heavily on inferences on the locations of loads as well as their respective distributions. One of the main limitations of this study comes from a lack of access to precise wind tunnel testing data and aircraft sizing requirements. A more accurate stability analysis can be completed with precise performance and sizing information from the aircraft manufacturer.

6. Fuel Consumption Analysis

With a 50% reduced empennage size in the CFJ model design, a projected empennage drag reduction of 50% was estimated. These results were validated using the aircraft performance and design methodology discussed in sections 3, and 4. As can be seen in table 7 above, the estimated 50% tail drag reduction is in good agreement with the calculated empennage drag reduction yielding a value of 57.17%. Accounting for decreased drag, the L/D in of the CFJ model increased by 4.88% in comparison to the baseline model.

A decreased structure weight coupled with increased aerodynamic efficiency yield significant improvements in fuel consumption for the B787-8 CFJ model. Referencing the take-off weight iterations, the fuel weight required for the aircraft was calculated accounting for the fuel weight fraction at every stage of the flight envelope. These calculations yield a required fuel weight of 19999.84, and 174041.28 lb. for the baseline and CFJ models respectively. The CFJ model experiences a 12.97% reduction in required fuel. Using a general conversion of 6.75 pounds per gallon for Jet A fuel [38], the total amount of gallons of fuel required for both models is calculated to be 29625.16 and 25783.89 gallons respectively. Considering statistics provided by the Bureau of Transportation, the estimated cost of commercial aviation fuel as of March 2023 is 2.91 USD per gallon [39] Due to the decreased weight and

improved aerodynamic performance, the B787-8 CFJ model effectively saves airlines an estimated 11,178.10$ on fuel per flight while preserving the baseline flight mission requirements.

7. Conclusion

This paper conducts a conceptual design study on the use of Coflow jet (CFJ) control surface technology on a Boeing 787-8 Dreamliner to allow for high surface control authority with a 50% reduced empennage size. The CFJ B787-8 model is designed with a 50% empennage size reduction, and a 10.24% wing size reduction. The design and analysis methodology applied in this study is validated using published aircraft performance and sizing parameters. The baseline calculated values yield percentage difference ranges from 0%-14% when compared to published aircraft. These values are within reasonable agreement with official data, effectively validating the design methodology applied within this study.

The horizontal and vertical tail components experience weight reductions of 50.94% and 47.75%. The weight of the CFJ actuator system is calculated based on a conservative power density of 3kw/kg and a conservative CFJ power efficiency of 75%. The horizontal and vertical CFJ component weight calculations yield a result of 891.43 lb. and 393.25 lb. With the CFJ subsystems considered, the horizontal and vertical tail weights still yield significant weight reductions of 32.4% and 31.9% respectively. The stability of the CFJ B787-8 is verified, with this study showing longitudinal and lateral stability are preserved with the reduced empennage size design,

With these aircraft component sizing and weight design parameters, the CFJ model shows a 4.65% decrease in total drag, and a 4.88% increase in L/D. The 50% reduced empennage design yields a 10.24% reduction in gross weight, and a 12.97% reduction in fuel weight. The conceptual study of this paper shows that CFJ empennage appears to be a promising technology which can allow for substantially reduced fuel consumption and emission pollution rates for transonic transports.

8. References

[1] IATA. (2022). *Fuel Fact Sheet* [Fact Sheet]. Retrieved October 10, 2022, from https://www.iata.org/en/iata-repository/pressroom/fact-sheets/fact-sheet---fuel/

[2] Anders, S., Sellers III, W., & Washburn, A. (2004). Active flow control activities at NASA Langley. *2nd AIAA Flow Control Conference*. doi:10.2514/6.2004-2623

[3] G.-C. Zha, B. F Carroll, C. D. Paxton, C. A. Conley, and A. Wells, "High-performance airfoil using coflow jet flow control," AIAA journal, vol. 45, no. 8, pp. 2087–2090, 2007, DOI: 10.2514/1.20926.

[4] Bower, W., & Kibens, V. (2004). An overview of active flow control applications at the Boeing Company. *2nd AIAA Flow Control Conference*. doi:10.2514/6.2004-2624

[5] Kandil, O., Gercek, E., Zheng, X., & Luo, X. (2004). Development of computational sensing and active flow control of airfoils during dynamic stall. *42nd AIAA Aerospace Sciences Meeting and Exhibit*. doi:10.2514/6.2004-43

[6] Lefebvre, A., Dano, B., Bartow, W. B., Difronzo, M., & Zha, G. C. (2016). Performance and energy expenditure of Coflow jet airfoil with variation of Mach number. *Journal of Aircraft, 53*(6), 1757-1767. doi:10.2514/1.c033113

[7] Van Buren, T., & Amitay, M. (2016). Comparison between finite-span steady and synthetic jets issued into a quiescent fluid. *Experimental Thermal and Fluid Science, 75*, 16-24. doi:10.1016/j.expthermflusci.2016.01.014

[8] Rathay, N. W., Boucher, M. J., Amitay, M., & Whalen, E. (2014). Performance enhancement of a vertical tail using synthetic jet actuators. *AIAA Journal, 52*(4), 810-820. doi:10.2514/1.j052645

[9] Lin, J. C., Andino, M. Y., Alexander, M. G., Whalen, E. A., Spoor, M. A., Tran, J. T., & Wygnanski, I. J. (2016). An overview of active flow control enhanced vertical tail technology development. *54th AIAA Aerospace Sciences Meeting*. doi:10.2514/6.2016-0056

[10] Andino, M. Y., Lin, J. C., Washburn, A. E., Whalen, E. A., Graff, E. C., & Wygnanski, I. J. (2015). Flow separation control on a full-scale vertical tail model using sweeping jet actuators. *53rd AIAA Aerospace Sciences Meeting*. doi:10.2514/6.2015-0785

[11] Seele, R., Graff, E., Gharib, M., Taubert, L., Lin, J., & Wygnanski, I. (2012). Improving rudder effectiveness with sweeping jet actuators. *6th AIAA Flow Control Conference*. doi:10.2514/6.2012-3244

[12] Seele, R., Graff, E., Lin, J., & Wygnanski, I. (2013). Performance enhancement of a vertical tail model with sweeping jet actuators. *51st AIAA Aerospace Sciences Meeting including the New Horizons Forum and Aerospace Exposition*. doi:10.2514/6.2013-411

[13] Rathay, N., Boucher, M., Amitay, M., & Whalen, E. (2014). Parametric study of synthetic-jet-based control for performance enhancement of a vertical tail. *AIAA Journal, 52*(11), 2440-2454. doi:10.2514/1.j052887

[14] E. Graff, R. Seele, J. C. Lin, and I. Wygnanski, "Sweeping jet actuators-a new design tool for high lift generation." 20130013994, *Innovative Control Effectors for Military Vehicles (AVT-215)*, Stockholm, Sweden, 20-22 May 2013.

[15] Shmilovich, A., Yadlin, Y., & Whalen, E. A. (2015). Computational evaluation of flow control for Enhanced Control Authority af a vertical tail. *33rd AIAA Applied Aerodynamics Conference*. doi:10.2514/6.2015-3311

[16] Kara, K. (2016). Numerical simulation of a sweeping jet actuator. *34th AIAA Applied Aerodynamics Conference*. doi:10.2514/6.2016-3261

[17] Kara, K. (2015). Numerical Study of internal flow structures in a sweeping jet actuator. *33rd AIAA Applied Aerodynamics Conference*. doi:10.2514/6.2015-2424

[18] Xu, K., & Zha, G. (2019). High Control Authority 3D aircraft control surfaces using Co-Flow Jet. *AIAA Aviation 2019 Forum*. doi:10.2514/6.2019-3168

[19] Pack, L., Schaeffler, N., Yao, C., & Seifert, A. (2002). Active control of flow separation from the slat shoulder of a supercritical airfoil. *1st Flow Control Conference*. doi:10.2514/6.2002-3156

[20] Xu, K., & Zha, G. (2022). 3D aircraft control surface enabled by Co-Flow Jet Flap. *AIAA AVIATION 2022 Forum*. doi:10.2514/6.2022-3889

[21] Xu, K., Zhang, J., & Zha, G. (2019). Drag minimization of co-flow jet control surfaces at cruise conditions. *AIAA Scitech 2019 Forum*. doi:10.2514/6.2019-1848

[22] Federal Aviation Association. *Air traffic by the numbers*. (n.d.). FAA. https://www.faa.gov/air_traffic/by_the_number

[23] International Air Transport Association. (n.d.). *Value of air cargo*. IATA. https://www.iata.org/en/programs/cargo/sustainability/benefits/

[24] Air Transport Action Group. (2022) *Facts & Figures* [Fact Sheet]. ATAG. https://www.atag.org/facts-figures/

[25] Norwegian Airlines. (2009). *Norwegian Boeing 787-8/9 Dreamliner*. Norwegian Airlines.

[26] Overton, J. (2022*). Issue brief: The growth in greenhouse gas emissions from Commercial Aviation* (2019, revised 2022). EESI. https://www.eesi.org/papers/view/fact-sheet-the-growth-in-greenhouse-gas-emissions-from-commercial-aviation

[27] Ahlgren, L. (2021, November 18). *Explained: The different types of Sustainable Aviation Fuel*. Simple Flying. https://simpleflying.com/sustainable-aviation-fuel-types/

[28] O'Callaghan, J. (2020, July 08). *Quiet and green: Why hydrogen planes could be the future of Aviation*. https://ec.europa.eu/research-and-innovation/en/horizon-magazine/quiet-and-green-why-hydrogen-planes-could-be-future-aviatio

[29] Corke, T. C. (2005). *Design of aircraft*. Pearson Education inc.

[30] Raymer, D. P. (1992). *Aircraft design: A conceptual approach*. AIAA.

[31] "Boeing 787-8 (Dreamliner) Sample Analysis. (2005)." Lissys, June 2006.

[32] Boeing. (2014). *787 Airplane Characteristics for Airport Planning*. Seattle , Washington; Boeing Commercial Airplanes .

[33] Ritchie, H. (2020, October 22). *Climate change and flying: What share of Global CO2 Emissions Come From Aviation?* https://ourworldindata.org/co2-emissions-from-aviation

[34] Le Feuvre, P. (2018, October 01). *Are aviation biofuels ready for take off? – analysis*. IEA. https://www.iea.org/commentaries/are-aviation-biofuels-ready-for-take-off

[35]European Union Aviation Safety Agency. (2019, April 30). *TYPE-CERTIFICATE DATA SHEET for Trent 1000 series engines*. EASA. https://www.easa.europa.eu/en/document-library/type-certificates/engine-cs-e/easae036-rolls-royce-deutschland-trent-1000-series

[36] *Powering the Dreamliner*. Trent 1000: Boeing 787 engine | Rolls-Royce. (n.d.). Retrieved April 8, 2023, from https://www.rolls-royce.com/products-and-services/civil-aerospace/widebody/trent-1000.aspx

[37] ForeFlight. (n.d.). *What fuel density does weight & balance use? – foreflight support*. Support Center. https://support.foreflight.com/hc/en-us/articles/6297854155159-What-fuel-density-does-Weight-Balance-use-

[38] Bureau of Transportation Statistic. (2023). *U.S. airlines' March 2023 fuel cost per gallon down 9.6% from February 2023; aviation fuel consumption up 1.3% from pre-pandemic March 2019*. BTS. https://www.bts.gov/newsroom/us-airlines-march-2023-fuel-cost-gallon-down-96-february-2023-aviation-fuel-consumption-13

[39] Detsios, N., Theodoraki, S., Maragoudaki, L., Atsonios, K., Grammelis, P., & Orfanoudakis, N. G. (2023). Recent advances on alternative aviation fuels/pathways: A critical review. *Energies*, *16*(4), 1904. https://doi.org/10.3390/en16041904

9. Appendix

9.1 Environmental and Economic Considerations

When investigating the effects of an active flow control system integration on the empennage, and its effects on aircraft flight performance, it is important to consider the economic and environmental considerations that come with it.

Aircraft transportation currently accounts for the majority of commercial travel. Optimization of aircraft performance over the years has allowed for a heavy reliance on air travel for commercial and economic purposes. Presently, figures estimate that approximately 45,000 flights occur daily over American airspace [22]. FAA records show an average of 29 million square miles of airspace is covered every day over the United States of America. At commercial aircraft peak in the year 2020, 16 million flights occurred within US airspace, and over 40 million flights occurred globally. Airlines have estimated a total of 4.5 billion passengers fly each year [22,24]. In addition to commercial applications, aircraft are estimated to carry 44.5 billion pounds of freight per year [22]. Aircraft freight transport only accounts for approximately 1% of the volume of world trade shipments, however, these shipments account for 35% of total trade shipment value [23]. Because of the high value worth of the goods transported via aircraft, freight flights significantly contribute to the global economy. Data from the International Civil Aviation Organization (IATA) show that freight flights contribute over 700 billion dollars on an annual basis [23] After the pandemic, air cargo E-commerce transported over 5 trillion dollars of goods and resources. Through the year 2022, 80% of cross-border e-commerce has been transported by air. With an ongoing demand increase, it is estimated that by the year 2040 95% of all purchases will be through air cargo e-commerce [23]

High reliance on air travel for both commercial travel and export has led to significant levels of greenhouse gas emissions. The international council on clean transportation estimates a total of 1.04 billion tons of CO2 emissions due to commercial aircraft flights, accounting for 2.5% of total global CO2 emissions per year [33]. Aircraft carbon emissions coupled with contrails lead to significant radiative forcing- where the radiative energy produced by aircraft exceeds that of incoming energy. Emissions due to aircraft travel account for approximately 3.5% of total anthropogenic warming [26,33]. While aircraft's ecological footprint is not as detrimental when compared to other contributors, a projected increase in flight occurrence can signal a potential exponentially increasing carbon footprint in the near future. Using current aircraft performance metrics, aircraft emissions on a national basis are estimated to increase by 3% over the coming years [26]. Such a stark projected increase in transport aircraft emissions has caused much concern among climate scientists about the potential impact air travel can have on the environment. In contrast to other sectors, the decarbonization of aircraft is limited due to the currently available fuel and energy sources. Historically, an increase in the fuel efficiency of aircraft has been achieved through aircraft design modifications. Since the 1950s, the aviation industry has seen a significant increase in air traffic volume by 300%; however, in recent years, slower emission growth has occurred despite a boom in air travel. This can be attributed to major developments and improvements in aviation efficiency [26].

The majority of current commercial and freight aircraft use traditional jet fuel for international flights. Over recent years, different aircraft fuel and energy sources have been researched showing possible fuel alternatives with less detrimental ecological implications. Sustainable Aviation fuels (SAF) such as Biofuels, and hydrogen fuel cells have been developed over the past few decades showing promising data concerning the future of air travel. Current first-generation biofuels reduce CO2 emissions compared to jet fuel by 50-80% over the product's life cycle [33,34,27]. These biofuels, also known as FOGs (fats, oils, and greases) marked the first step in decreasing aircraft greenhouse gas emissions. Further fuel development and research have led to the creation of biomass and Municipal solid waste (MSW) derived fuels [33,34]. These second-generation biofuels are created from algae, crop residue, animal waste, and forestry residue. The performance of MSW biofuels exceeds that of FOGs, with a higher potential reduction of greenhouse gas emissions by 85-95% over the aircraft life cycle compared to conventional jet fuel [27]. The use of biofuel is one of the most viable options to reach a target of reducing carbon

emissions by 50% by 2050 [33,27]. While the use of biofuels can lead to significant carbon emission reduction, there has not been enough development to support the consistent use of biofuels over conventional fuel. The main limiting factor when considering the use of biofuels in commercial air travel comes from the overall operational cost, as well as fuel availability. The current market for biofuels is not large enough to trigger enough fuel production to support most transport flights. There are currently less than five airports in the entire world that hold a consistent supply of biofuels [33,34]. A limited biofuel supply coupled with high production costs make biofuels much less cost-effective than conventional fuel alternatives [33]. With aircraft fueling accounting for the largest overhead expense for airlines, the use of more expensive biofuels is not as attractive to commercial airlines. Until the biofuel market experiences a significant increase, it is not expected that airlines will adopt such an alternative.

In addition to biofuels, hydrogen fuel is widely considered a viable ecologically friendly alternative to traditional jet fuel. Hydrogen is a clean fuel that converts hydrogen to electricity, subsequently only emitting water, effectively being the only fuel source with a net-zero carbon footprint potential. Hydrogen fuel has been cited to have made even more promising performance metrics than that of biofuels. Hydrogen-fueled aircraft is comprised of a storage system, fuel cells to produce electricity, a motor, and a power control device for the cells [28]. This is an aircraft component deviation from conventional aircraft, making it so sufficient development in all these components is necessary to produce hydrogen-electric aircraft. To support a hydrogen-fuel system, aircraft must undergo significant redesign. Significant development is still needed in all these subsystems to support a hydrogen-fueled aircraft. State-of-the-art hydrogen fuel cell technology currently supports short-range single-passenger aircraft. It is expected that hydrogen fuel powered short-range (<1600 Nautical Miles) aircraft could be used by the year 2035, and medium-range (<3800 Nautical Miles) aircraft by the year 2040 [28]. A lot more research and development is needed for hydrogen-fuel system integration into long-range transport aircraft. In addition to this, to fully benefit from the use of hydrogen fuel, clean hydrogen needs to be mass-produced, and distributed. Currently, the majority of hydrogen is being produced from fossil fuels, in order to achieve a net zero carbon footprint, the production of clean hydrogen from water must become the leading production source of the fuel. Similarly, to Biofuels, there is still much development research needed to be done to normalize the use of hydrogen fuel [28].

9.2 B787 Aircraft Design Parameters (Continued)

Aircraft design methodologies were derived from Corke and Raymer design books [29,30].

9.2.1 Wing Drag Estimation

The wing drag calculation is the summation of the base drag, the lift-induced drag, and the losses due to flow separation. The drag estimation is related to its respective drag coefficient.

$$C_D = C_{D\circ} + kC_L{}^2 + k'(C_L - C_{Lmin}) \tag{62}$$

Assuming that the drag bucket encompasses the Cl range throughout cruise, then the losses due to separation can be assumed to be zero.

$$C_D = C_{D\circ} + \ kC_L{}^2 \tag{63}$$

Using Oswald's wing efficiency factor, the fuselage and taper ratio effects are accounted for in the lift-induced drag calculations. The fuselage diameter to wingspan ratio and an estimated Oswald efficiency factor of .8

$$k = \frac{1}{\pi Ae} \tag{64}$$

$$e = e'\left[1 - \left(\frac{d}{b}\right)^2\right] \tag{65}$$

The zero-lift drag coefficient accounts for viscous skin friction drag caused by flow separation. The 3-dimensional zero-lift drag coefficient can be estimated with the viscous drag coefficient. The friction coefficient is used for the calculation of viscous drag on the surface. Depending on the development length of the flow boundary layer, the friction coefficient for laminar and turbulent flow is calculated.

$$cf = \frac{1.328}{\sqrt{Re_x}} : laminar \tag{66}$$

$$cf = \frac{.455}{(log_{10} * Re_x)^{2.58}(1+.144*M^2)^{.65}} : turbulent \left(\sqrt{Re_x} \geq 1000\right) \tag{67}$$

To correct for possible imperfections on a 3-dimensional wing, the form and interference factors can be used. In considering flow separation, the form factor is used to determine the increase in the friction coefficient.

$$F = \left[1 + \frac{.6}{\left(\frac{x}{c}\right)_m}\left[\frac{t}{c}\right] + 100\left[\frac{t}{c}\right]^4\right]\left[1.34M^{,18}\left(cos\left(\Lambda_{\frac{t}{c}max}\right)\right)^{.28}\right] \tag{68}$$

The interference factor estimates the increase in base drag due to structural interference by the fuselage or aircraft attachments. This value is dependent on attachment configuration and placement. The interference factor used for the purpose of this study is given a value of 1.

$$C_{D\circ} = C_f * F * Q * s_{\frac{wet}{S}} \tag{69}$$

9.2.2 Fuselage drag estimation

The Boeing 787-8 is a subsonic aircraft, making it so the only major drag effect is that due to viscous effects.

$$F_f = qSC_f \tag{70}$$

The above equation denotes viscous drag acting on the fuselage, with q being the dynamic pressure at cruise conditions, S being the surface area of the fuselage, and Cf the friction coefficient. The wetted area of the aircraft can be calculated using the incremental shape dimensions of the fuselage [29].

$$S = \sum_1^N P_i x_i \tag{71}$$

Where the fuselage is divided into N pieces and the area can be calculated by adding the products of the perimeter and x coordinate across the fuselage profile. The friction coefficient is calculated based on the Reynolds number of the flow, with the outer edge boundary layer velocity, the development length on the x-axis, and the dynamic viscosity [29].

$$Re_x = \frac{U_o x}{v} \tag{72}$$

$$C_f = \frac{1.38}{\sqrt{Re_x}} \quad : For\ Laminar\ flow \tag{73}$$

$$C_f = \frac{.455}{(ln\,(Re_x))^{2.58}(1+0.144M^2)^{0.65}} \quad : For\ Turbulent\ flow\ \sqrt{Re_x} \geq 1000) \tag{74}$$

The fuselage form factor is given by the following equation. With f being the inverse fineness ratio (l/d) [29]

$$F = 1 + \frac{60}{f^3} + \frac{f}{100} \tag{75}$$

The total viscous drag on the fuselage is calculated as seen below [29]

$$F_f = qSC_fFQ \tag{76}$$

With the interference factor being negligible, an approximation of Q=1 can be made [29]

9.2.3 Structure Weight

The following relations are used in the structure component weight calculations for the aircraft as derived by Corke and Raymer. [29,30]

$$W_{Wing} = .0051(W_{dg}n)^{.557}(S_W)^{.649}(A)^{.5}(\frac{t}{c})^{-.4}(1+\lambda)^{.1}(cos\ (\Lambda))^{-1}(S_{csw})^{.1} \tag{77}$$

A K_{lg} value of 1.12 is used for fuselage mounted landing gear, The Boeing 787-8 has a non-delta wing design thus a value of 1 is used to denote K_{dwf}. The aircraft is equipped with two side cargo doors and an aft clamshell door therefore 1.25 is used to denote K_{door} [30]

$$W_{Fuselage} = .328K_{door}K_{lg}(W_{dg}n)^{.5}(S_f)^{.302}(L_f)^{.25}(1+K_{ws})^{.04}(\frac{L}{D})^{.1} \tag{78}$$

The wing sweep factor, K_{ws} ,is quantified as seen below [30].

$$K_{ws} = .75[(1+2\lambda)/(1+\lambda)](\frac{B_w}{L})(tan\ (\Lambda) \tag{79}$$

The landing gear weights are calculated using a value of 1 for K_{np} to denote a non-kneeling gear. There are two nose wheels on the Dreamliner, thus 2 is used for N_{nw} [30].

$$W_{Landing} = .03K_{np}(L_n)^{.65}(N_{nw})^{.5}(W_l)^{.45} \tag{80}$$

The nacelles on the aircraft are pylon mounted, thus a value of 1.017 is used for K_{ng} in the nacelle group weight calculation. The engine considered in this study is the Rolls Royce Trent 1000, with a single engine dry weight of 13,087 lb, a length of 15.4 ft, a width of 9.33 ft, and a wetted area of 1457.93 ft2 [35]. The Boeing 787-8 is a twin jet aircraft, therefore two engines are considered in these calculations.

$$W_{Nacelle} = .6724K_{ng}(N_{lt})^{.1}(N_W)^{.294}(N_Z)^{.119}(W_{ec})^{.611}(N_{en})^{.984}(S_n)^{.224} \tag{81}$$

The engine control, pneumatic system, and fuel system weights are calculated in the following equations [30].

$$W_{Engine\ control} = .8L_{np} + .5N_{en} \tag{82}$$

$$W_{Pneumatic} = 49.19(\frac{W_{en}N_{en}}{1000})^{.541} \tag{83}$$

$$W_{Fuel\ System} = .03K_{np}(L_n)^{.65}(N_{nw})^{.5}(W_l)^{.45} \tag{84}$$

$$W_{Fuel\ system} = 2.405(V_t)^{.606}(1+\left(\frac{V_i}{V_t}\right)^{-1}\quad\left(1+\left(\frac{V_p}{V_t}\right)\right)(N_t)^{.5} \tag{85}$$

The total number of separate actions controlled by surfaces by the Boeing 787-8 is 7, therefore the value assigned to N_f is 7 [30].

$$W_{Flight\ control} = 145.9(N_f)^{.554}\left(1 + \left(\frac{N_m}{N_f}\right)^{-1}\right)(S_{cs})^{.2}\,(I_{Yaw} * 10^{-6})^{.07} \tag{86}$$

The following equation denotes the yawing moment of inertia calculated for the aircraft [30].

$$I_{Yaw} = \frac{(\frac{B_w + L_f}{2})^2\left(W_{dg}(.46^2)\right)}{4*32.17} \tag{87}$$

$$W_{APU\ Installed} = 2.2(W_{APU\ uninstalled}) \tag{88}$$

In the weight estimation for the instruments, a value of 1 is used for K_r and K_{tp}, to denote the aircraft engines are not reciprocating or turboprop. There is an estimated 10 crew members accounted for, thus this value is used in denoting N_c [30].

$$W_{Instruments} = 4.509(K_r K_{tp})\ \ (N_c)^{.541}(N_{en})\left(L_f + B_w\right)^{.937} \tag{89}$$

$$W_{Hydraulics} = .2673(N_f)\left(B_w + L_f\right)^{.937} \tag{90}$$

$$W_{electrical} = 7.291(R_{kva})^{.782}\,(L_a)^{.346}N_{en}^{.1} \tag{91}$$

$$W_{avionics} = 1.73(W_{uav})^{.983} \tag{92}$$

$$W_{furnishing} = .0577(S_f)^{.75}\,(N_c)^{.1}(W_c)^{.393} \tag{93}$$

For the purpose of this study, the furnishing weight is also deduced from online B787-8 analysis [31,30].

$$W_{air\ conditioning} = 62.36(N_p)^{.25}\left(\frac{V_{pr}}{1000}\right)^{.604}(W_{UAV})^{.1} \tag{94}$$

$$W_{Handling\ gear} = 3 * 10^{-4}\left(W_{dg}\right) \tag{95}$$

$$W_{Anti-Ice} = .0002\left(W_{dg}\right) \tag{96}$$